Title: SARS-CoV-2 induces acute neurological signs while Calcitonin Gene-Related Peptide (CGRP) signaling blockade reduces interleukin 6 (IL-6) release and weight loss in mouse models.

Abbreviated title: SARS-CoV-2 induces acute neurological signs while CGRP signaling blockade reduces interleukin 6 (IL-6) release and weight loss

Authors: Shafaqat.M. Rahman [1,co], David W. Buchholz[2,co], Brian Imbiakha.[2,co], Mason.C. Jager[3], Justin Leach, [1], Raven.M. Osborn [1], Ann O. Birmingham [1], Stephen Dewhurst[1], Hector C. Aguilar [2,*] , and Anne E. Luebke, [1,*]

Affiliations:

[1]University of Rochester Medical Center, Departments of Biomedical Engineering, Neuroscience, Microbiology and Immunology, Rochester, NY, USA;

[2] Cornell University, Department of Microbiology and Immunology, College of Veterinary Medicine, Ithaca, NY, USA.

[3] Cornell University, Department of Population Medicine, College of Veterinary Medicine, Ithaca, NY, USA.

[co] Contributed equally

*Send correspondence to: Anne E. Luebke (aluebke@ur.rochester.edu) or Hector C. Aguilar (haguilar@cornell.edu)

Submitting author: Anne E. Luebke (aluebke@ur.rochester.edu)

Number of Pages: 29

Number of Figures: 6

Number of Tables: 0

27 **Number of words for Abstract:** 151

28 **Number of words for Significance Statement:** 102

29 **Number of words for Introduction:** 552

30 **Number of words for Discussion:** 332

31 **Conflict of interest statement:** The authors declare no competing financial interests.

32 **Acknowledgments**: This research is supported by a COVID-19 research supplement to NIH R01

33 DC017261 (AEL). We would also like to thank Dr. Ralph S. Baric (UNC) for the MA-10 SARS

34 CoV-2 virus stock, the BSL3 facility and staff in the Center for Advanced Research

35 Technologies at the University of Rochester, and the ABSL3 facility and staff at Cornell

36 University. We would also like to thank Shruti Aryal for assisting with data analysis.

Abstract:

COVID-19 can result in neurological symptoms such as fever, headache, dizziness, and nausea. We evaluated whether the Calcitonin Gene-Related Peptide (CGRP) receptor antagonist, olcegepant, used in migraine treatment could mitigate acute neuroinflammatory and neurological responses to SARS-COV-2 infection. We infected wildtype C57BL/6J and 129/SvEv mice, and a 129 αCGRP-null mouse line with a mouse-adapted SARS-CoV-2 virus, and evaluated the effect of CGRP receptor antagonism on the outcome of that infection. We determined that CGRP receptor antagonism provided protection from permanent weight loss in older (>12 m) C57BL/6J and 129 SvEv mice. We also observed acute fever and motion-induced dizziness in all older mice, regardless of treatment. However, in both wildtype mouse lines, CGRP antagonism reduced acute interleukin 6 (IL-6) levels by half, with virtually no IL-6 release in mice lacking αCGRP. These findings suggest that blockage of CGRP signaling protects against acute IL-6 release and subsequent inflammatory events after SARS-CoV-2 infection.

Significance Statement:

COVID-19 can cause neurological symptoms such as fever, headache, dizziness, and nausea. However, such neurological symptoms of SARS-CoV-2 infection have not been assessed in mouse models. Here, we infected two commonly used wildtype mice lines (C57BL/6 and 129S) with mouse-adapted SARS-CoV-2 – and demonstrated neurological signs that including motion-related dizziness. Further, we show that CGRP signaling blockade can reduce IL-6 release and reverse long-term weight loss associated with SARS-CoV-2 infection, without rescuing either fever and dizziness. These findings suggest that CGRP signaling blockade can be protective in acute SARS-CoV-2 infections, and raise the possibility that it may also impact long-term outcomes of infection.

Introduction

Coronavirus disease (COVID-19) caused by severe acute respiratory syndrome CoV-2 (SARS-CoV-2) has caused a 3-year, ongoing, world pandemic (Zhu et al. 2020). There is a sound premise supporting testing CGRP-receptor antagonists such as olcegepant as a way to mitigate the neuroimmune consequences of SARS-CoV-2 infection (Robertson 2020). While CGRP has pleotropic effects on the immune system, CGRP release occurs as a result of SARS-CoV-2 activation of the transient receptor potential (TRP) channels; and is implicated in COVID-19 neurological symptoms such as fever, headache, dizziness, nausea pain, and the subsequent release of interleukin 6 (IL-6) (Assas, Miyan, and Pennock 2014; Assas, Pennock, and Miyan 2014; Channappanavar and Perlman 2017). IL-6 is an important mediator of inflammation that is often elevated in severe COVID-19 infection, and may be involved in the hyperimmune response cascade (cytokine storm) and the polarization of T-cell responses (Aghagoli et al. 2021; Liu et al. 2020). Headache, nausea, and dizziness are common neurological manifestations of COVID-19 infection (Bohn et al. 2020; Saniasiaya and Kulasegarah 2021) and in COVID-19 patients headache severity has been correlated with IL-6 levels (Bolay et al. 2021; Karadas et al. 2021).

Studies have shown that both SARS-CoV-1 (2002 outbreak) and SARS-CoV-2 (2019 outbreak) enter the body by binding to the angiotensin-converting enzyme 2 (ACE2) cell receptor (Kuba et al. 2005; Ziegler et al. 2020). However, due to sequence and structural differences between mouse ACE2 and human ACE2, human SARS coronaviruses exhibit a species-restricted tropism and are inefficient at infecting wild-type mice. To overcome this obstacle, the Baric laboratory modified the clinical SARS-CoV-2/USA-WA1 variant to gain the ability to bind to the murine ACE2 receptor after serial passaging in mice, to generate the MA10-SARS-CoV-2 virus (Dinnon et al. 2020, 2021); we used this mouse-adapted virus in most of our study.

90 We first assessed both neurological symptoms of fever and dizziness/nausea in mouse models
91 after infection with the MA10-SARS-CoV-2 virus. As a readout of the nausea-like state present
92 after SARS-CoV-2 infection, we examined hypothermic responses to provocative motion, as we
93 have previously used to assess migraine nausea pain (Biorxiv
94 doi.org/10.1101/2022.06.03.494762). Studies have demonstrated that provocative motion
95 causes robust and prominent hypothermic responses in rats, humans, house musk shrews, and
96 mice. These decreases in body temperature can represent a biomarker of a nausea-like state in
97 laboratory animals as: i) temperature changes are provoked both by motion and by chemical
98 emetic stimuli, ii) differential pharmacological sensitivity of these responses mirrors sensitivity in
99 humans, iii) motion-induced hypothermia *precedes* emetic (vomiting) episodes, and iv) there is a
100 clear parallel in hypothermic responses between animals and humans in underlying
101 physiological mechanism - cutaneous vasodilatation that favors heat loss (Del Vecchio et al.
102 2014; Mazloumi Gavgani, Hodgson, and Nalivaiko 2017; Ngampramuan et al. 2014; Romano et
103 al. 2017; Tu et al. 2017). In the nausea/dizziness assay after provocative motion there is a
104 decrease in head temperature and an increase in tail temperature. We have shown that in
105 wildtype C57BL/6Jmice injection of Calcitonin Gene-Related Peptide (CGRP) prolongs this
106 head temperature response and blunts the transient tail temperature increase, whereas a
107 CGRP-receptor antagonist can reverse these CGRP-induced changes (Doods et al. 2000;
108 Mallee et al. 2002) and Biorxiv doi.org/10.1101/2022.06.03.494762. Therefore, we investigated
109 if a MA10-SARS-CoV-2 viral infection would show similar acute dizziness/nausea responses as
110 CGRP injection, and if antagonizing CGRP signaling could reduce these dizziness/nausea
111 responses.
112

113 **Materials and Methods**

114 **Animals**

115 A total of 180 mice (120 M/60F) were used in these studies, either 129SvEv (Taconic
116 129SVE) or C57B6/J (JAX 0664) or αCGRP (-/-) null mice on a 129SvEv background. Prior to
117 SARS-CoV-2 infection, mice were bred and housed under a 12 to 12 day/night cycle at the
118 University of Rochester 's Vivarium under the care of the University of Rochester's Veterinary
119 Services personnel. Mice were implanted with transponder chips (Backagin Microchip FDX-B
120 ISO 11784/11785) to allow for blinded identification; and when relevant, implanted with pellets
121 containing placebo or olcegepant (BIBN4096, Tocris; 2 mg/kg/day/SQ; Innovative Research of
122 America, Inc.). After pretesting was performed, mice were transferred to Cornell's ABSL3
123 facility, and acclimated prior to virus infection and testing. All animal procedures were approved
124 both by the University of Rochester's and Cornell University's IACUC committees and
125 performed in accordance with NIH standards.

126

127 **Virus propagation**

128 Vero-E6 cells (obtained through BEI resources, NIAID, NIH, NR-53726) were cultured in
129 Eagle's Minimum Essential Medium (ATCC, #30-2003) supplemented with 10% (vol/vol) fetal
130 bovine serum (FBS) (Gibco, CA) and 1% penicillin-streptomycin (Pen-Strep, Life Technologies)
131 at 37°C in a 5% (vol/vol) CO_2 atmosphere. Viral stocks of mouse-adapted SARS-CoV-2 (MA10)
132 (obtained from the laboratory Dr. Ralph Baric) were propagated in Vero-E6 cells in 2% (vol/vol)
133 FBS and 1% penicillin-streptomycin at 37°C at a multiplicity of infection (MOI) of 0.1. Viral stock
134 titers were determined by $TCID_{50}$ analysis. Viral propagation involving live SARS-CoV-2 was
135 conducted in Biosafety level 3 (BSL3) facilities both at the University of Rochester and at
136 Cornell University.

137

138 **Animal Biosafety level 3 (ABSL3) facility and viral inoculations**

139 Mice were anesthetized using isoflurane and subsequently intranasally infected with MA-
140 10 SARS-CoV-2. For infection with live virus, drops of the pre-characterized viral stock were
141 administered into the rostral meatus of the nose, with a total volume of 50 µL per mouse. Daily
142 monitoring and weighing of the mice were conducted until they reached a predetermined
143 humane endpoint of 20% weight loss from their starting weight and/or severe clinical signs, at
144 which point animals were humanely euthanized. Mouse studies were conducted in a BSL-3
145 laboratory and in accordance with protocols approved by the Institutional Animal Care and Use
146 Committee at Cornell University (IACUC mouse protocol # 2017-0108 and BSL3 IBC # MUA-
147 16371-1). See Fig. 1A.

148

149 **Motion-Induced Thermoregulation Testing**

150 Tu et al. first noticed thermoregulatory changes in the temperatures of the heads,
151 bodies, and tails of mice, in response to provocative motion (Tu et al. 2017) . We therefore
152 adapted their protocol for the present study (Biorxiv doi.org/10.1101/2022.06.03.494762).
153 Head and tail temperatures of C57B6/J mice were measured for a total of 45 minutes using a
154 FLIR E60 IR camera (model: E64501), as depicted in Fig. 1A. This camera was connected to a
155 tripod and positioned approximately 43 cm above an open, plexiglass box (mouse box) used to
156 house an individual mouse during testing. Both the tripod and mouse box were securely
157 attached to the shaker's base. Briefly, baseline measurements were recorded for five minutes
158 prior to the provocative motion (-5 to 0 mins). The provocative motion was an orbital rotation (75
159 rpm, 2-cm orbital displacement), and mice were video-recorded for 20 minutes (0 to 20 mins).
160 After 20 minutes, the provocative motion was turned off, and mice were video-recorded for an
161 additional 20 minutes to measure recovery to baseline (20 to 40 mins) as schematized in Figs.
162 1A and 2. Head and tail temperatures were measured after data retrieval using the software
163 FLIR Tools+. Tail and head temperatures were measured within predefined field of views:

164 square region (3x3 mm) for tail, and circular region (10x10 mm) for head. Tail measurements
165 occurred 2 cm from the base of the tail and head measurements occurred at the center of the
166 head image, in between the mouse's ears. Infrared imaging data was collected every minute
167 during baseline measurements, and every 2 minutes during and after the provocative motion.
168 We quantified thermoregulatory changes to provocative motion by comparing changes in tail
169 vasodilatations, and we approximated the magnitude of the head hypothermia based on second
170 order curve fit estimates. Transient increases in the tail temperature of the mouse to provocative
171 motion are referred to as Δ *tail vasodilatations* (^{o}C), and were computed by subtracting the tail
172 temperature at time t = 0 minutes (rotation ON) from the max tail temperature measured during
173 the first 10 mins of the rotation ($0 \leq t \leq 10$).

174

175 **Pulse Oximetry**

176 A mouse Stat Jr X (Kent Scientific) was used to measure oxygen saturation (O2%) of
177 mice (see Fig. 1B). The O_2 sensor was applied to the rear leg, and data were recorded following
178 readout stabilization, defined as an unchanging recording over 5 seconds.

179

180 **BAL harvest and tissue processing**

181 Mice were euthanized with CO_2 , and bronco-alveolar lavage BAL fluid was removed
182 from the lung; animals then underwent laparotomy and sternotomy with subsequent left and
183 right ventricular cardiac perfusion with 20 mL total of PBS. Lungs were treated with 4%
184 paraformaldehyde/PBS (volume/volume) for a minimum of 72 hours to ensure full viral
185 inactivation. Tissues were taken out of the BSL3 facility and underwent dehydration with ethanol
186 and were later embedded in paraffin blocks for histological analysis.

187

188 **Histopathology**

189 For histological examination, mouse lungs were collected directly after euthanasia and
190 placed in 10% neutral buffered formalin for 72 h, after which tissues were embedded in paraffin.
191 Four-micrometer tissue sections were stained with hematoxylin for analysis.
192 Immunohistochemistry and digital image analysis for SARS-CoV-2 nucleocapsid was performed
193 as previously described (Shapira et al. 2022). Briefly, 4 μm tissue sections were labeled with a
194 rabbit IgG monoclonal antibody against SARS-CoV-2 nucleocapsid protein (GeneTex;
195 GTX635679) at a 1:5,000 dilution and processed using a Leica Bond Max automated IHC
196 Stainer. Digital image analysis was performed using QuPath software v.0.2.3 (Achanta et al.
197 2012; Bankhead et al. 2017; Shapira et al. 2022; Shapira et al. 2021).

198

199 **Imaging**

200 Histological specimens were visualized using a Zeiss Axioplan 2 microscope.
201 Immunohistochemistry (IHC) and hematoxylin and eosin (HE) stained slides for each specimen
202 were photographed in sequential order. In Adobe Photoshop, all images were sized with a
203 2080x2080 pixel frame and cropped to a uniform resolution of 1500x1500 pixels. IHC images
204 were further analyzed using Color Selection and Magic Wand tools where areas containing
205 brown staining were manually selected and cut into a separate layer. All images were exported
206 into JPEG format. For staining percentages, quantification was performed using ImageJ.
207 Images were converted from RGB Color into 8-bit grayscale and made Binary to set an
208 automated threshold. Area was then calculated with the Analyze Particles function. Circularity of
209 staining was assessed using the Circularity parameter set to 0.9-1.0.

210 **Quantification of lavage cytokines by ELISA**

211 Immulux 4HBx plates (ThermoFisher Scientific, #3855) were coated with IL-6 capture
212 antibody (ThermoFisher Scientific, MP5-20F3) and left overnight at 4°C. Wells were washed five

213 times with PBS+0.05% Tween 20 and blocked with PBS+5% dry milk solution (Bio-Rad,
214 1706404) for 1 hour at room temperature. 50µL of lavage sample or standard (R&D systems,
215 406-ML-005/CF) was added to the blocked wells for 2 hours at room temperature. Bound
216 cytokine was detected using a biotinylated IL-6 detection antibody (ThermoFisher Scientific,
217 MP5-32C11), streptavidin horseradish peroxidase (strep-HRP), and tetramethylbenzidine (TMB)
218 (ThermoFisher Scientific, 34028). Wells were washed three times following the addition of
219 detection antibody and strep-HRP. Reactions were stopped with 2N H_2SO_4 and ODs were read
220 at 450nm. Cytokine concentrations for each sample were determined by plotting OD values on a
221 standard curve using IL-6 recombinant protein. All testing was performed in triplicate.

222

223 **Statistics**

224 Two-way mixed effects (ME) models were used to assess % weight loss, and core
225 temperatures (^{o}C) across the factors: i) placebo vs olcegepant protection and ii) dpi. Two-way
226 ME models were also used to assess: i) viral infection vs pretest and ii) placebo vs olcegepant
227 protection for tail vasodilation responses at 3 dpi. Bonferroni multiple comparisons test was the
228 preferred post-hoc analysis method. X-intercept analyses of head recovery (mins) were
229 conducted assuming a quadratic model, least squares regression fitting, and constraints where
230 the x-intercept must be greater than x = 20 mins and the curve fit was approximated to x = 50
231 mins. Nested 1-way ANOVAs with Tukey post hoc was used to analyze BAL IL-6
232 concentrations and H&E staining (positive SARS-CoV-2 cells per mm^2).

233

234

235 **Results**

236 **MA-10 SARS-CoV-2 infection induces a fever-like state and disrupts**
237 **thermoregulation to provocative motion.** We measured baseline head temperatures in 18
238 month-old male /6J, 129SvEv, and 129 αCGRP-null groups of mice during pretesting and 3

239 days post-infection (dpi) with 10^5 pfu of MA-10 SARS-CoV-2 virus (**Fig. 2A&B**). Our results
240 showed a higher head temperature at 3 dpi, indicating a fever in all mice, regardless of strain
241 and olcegepant pretreatment (**Fig. 2B**).

242 We also measured motion-induced thermoregulation and weight changes in 18 month-
243 old male C57BL/6J, 129SvEv, and 129 αCGRP-null groups of mice at 3 dpi with 10^5 pfu of MA-
244 10 SARS-CoV-2 virus (**Fig. 3A**). Motion-induced thermoregulation was pre-tested in each
245 mouse 5-7 days prior to the infection. During the pre-test, we observed transient tail vasodilation
246 in response to provocative, nauseating stimuli (**Fig 3B,C,D**). The assay involved a 5-minute
247 baseline recording, a 20-minute rotation period (75 rpm, 1 cm orbital displacement), and a 20-
248 minute recovery period (as shown in **Figs. 1B and 3A**). Tail temperature profiles also indicated
249 a fever-like state after infection with MA-10 SARS-CoV-2, with higher tail temperatures at all
250 time points during the 3 dpi test than during the pretest (**Fig. 3B,C,D**). We computed a shift in
251 the Δ tail vasodilations by subtracting the magnitude of Δ tail vasodilations at 3 dpi from an
252 animal's pretest Δ tail vasodilation. With the exception of infected αCGRP-null mice, we
253 observed a decrease in the magnitude of tail vasodilations in infected mice compared to their
254 pretest, as indicated by a negative change in the Δ tail vasodilation - which is a sign of less
255 severe dizziness.

256 Typically, a twenty-minute provocative rotation in mice causes observable hypothermia,
257 and an additional 20-minute recovery period is needed for the mice to recover to their baseline
258 head temperature. Interestingly, we observed that viral infection delayed this recovery period, as
259 seen in our raw data (**Fig. 3 E,F,G**). Using a second-order polynomial fit ($B_0 + B_1X + B_2X^2$), we
260 estimated the time required for the mice to recover back to their baseline head temperature by
261 interpolating a curve fit to t = 50 minutes (**Fig. 3H).** We then computed a Δ head recovery by
262 subtracting the recovery period at 3 dpi from the pretest, where a positive Δ head recovery
263 indicated a longer recovery period due to the infection. In all infected males, regardless of
264 olcegepant treatment or strain, we observed a longer recovery period at 3 dpi ($p < 0.0001$). No

265 protective effects were seen by olcegepant in head temperature recovery for either strain (**Fig.**
266 **3H**).

267

268 **Olcegepant blockage or developmental loss of CGRP receptor leads to reduced IL-6**
269 **production in response to MA-10 infection**

270 SARS-CoV-2 infected 129/SvEv mice treated with olcegepant pellets had lower
271 interleukin 6 (IL-6) concentrations in their bronchoalveolar lavage (BAL) as compared to mice
272 treated with placebo (**Fig. 4B**). Congruently, the lower IL-6 concentrations in olcegepant-treated
273 mice were similar to the IL-6 concentrations measured in the αCGRP-null (-/-) mice (**Fig 4B**),
274 which is consistent with the relationship between CGRP and IL-6 levels in migraines (Han
275 2019). In C57BL/6J mice, similar observations regarding olcegepant's effects in reducing IL-6
276 post-infection were observed but did not reach statistical significance (**Fig 4A**).

277 **Older mice treated with olcegepant recovered from the initial weight loss by 7 dpi.**

278 When 18-month-old C57 or 129S mice were infected with MA-10, those pretreated with
279 olcegepant pellets showed a faster recovery to baseline weight compared to mice that received
280 placebo pellets. This effect was observed in both female and male C57BL/6J mice (**Fig. 5A**), as
281 well as in older female and male 129SvEv mice (**Fig. 5B**). Notably, 129S αCGRP (-/-) null mice
282 of either sex experienced similar trends as 129S WT mice given olcegepant (**Fig. 5E**). Older
283 infected mice exhibited lower core temperatures compared to the uninfected groups; however,
284 olcegepant had no distinguishable effect on core temperatures regardless of age or strain (**Fig.**
285 **5 B,D,F**). In addition, MA-10 infection did not significantly impact O_2% saturation in mice
286 regardless of age, sex, or strain. However αCGRP-null mice exhibited lower weight loss trends
287 following virus infection that did WT mice - suggesting that the αCGRP-null mice have a
288 reduced sensitivity to the MA-10 virus.

289 Histological analysis of lung tissue revealed no significant differences in the number of
290 SARS-CoV-2 infected cells in the lungs of C57BL/6J or 129S WT mice at 3 dpi (**Fig. 6 A&B**).
291 However, olcegepant-protected mice and αCGRP-null mice showed reduced staining for SARS-
292 CoV-2 when compared to placebo-treated mice, and this observation correlated with IL-6 levels.
293 **Fig. 6 C&D** shows SARS-CoV-2 staining (scale = 100 μm) of C57BL/6J (**C**) and 129S (**D**) lung
294 tissues.

295

296

297 **Discussion:**

298 Early in the pandemic, there was a controversy as to whether CGRP plasma levels were
299 increased or decreased in COVID-19 disease (Abobaker and Darrat 2021; Ochoa-Callejero et
300 al. 2021). However, a recent study with a relatively greater number of patients showed that
301 elevated CGRP plasma levels are correlated with increased disease severity in hospitalized
302 COVID-19 patients (Rizzi et al. 2022). In our study, the migraine drug olcegepant (small
303 molecule CGRP receptor antagonist) reduced IL-6 release at three days post-infection (3 dpi) in
304 two distinct wildtype mouse strains (C57B6 and 129S). Interestingly however, there was not a
305 similar protective effect on fever or on the dizziness/nausea-like state elicited by SARS-CoV-2
306 MA-10 in these same infected mice, as tested at 3 dpi.

307 A few studies have investigated CGRP antagonism on individuals infected with SARS-
308 CoV-2. In one study (Caronna et al. 2021), no deleterious effects of CGRP antagonism were
309 found, and no differences in symptom severity were found between CGRP antagonism to other
310 treatment modalities in migraine subjects. However, in this study, patients were not stratified by
311 age. We observed CGRP antagonism was protective from weight loss and IL-6 release only in
312 older mice. COVID-19 symptoms are more severe and mortality rates are higher in aged
313 human patients, adding significance to our results. Further, two relatively recent case studies
314 showed that increased headaches after SARS-CoV-2 infection can be treated with CGRP
315 monoclonal antibodies (Grassini et al. 2021; Ozkan et al. 2022). Our study suggests that
316 olcegepant or other CGRP treatments may be further explored particularly to treat headaches or
317 migraines in aged individuals and/or those with high IL-6 levels upon COVID-19 infection.

318 In conclusion, in addition to the acute effects studied here, antagonizing CGRP signaling
319 may be therapeutic against long COVID, as long COVID patients also show higher IL-6 plasma
320 levels (Littlefield et al. 2022). As long COVID has been demonstrated in mouse models (Dinnon
321 et al. 2022), future plans include investigating if antagonizing CGRP signaling in preclinical
322 models can mitigate neurological long COVID symptoms.

323

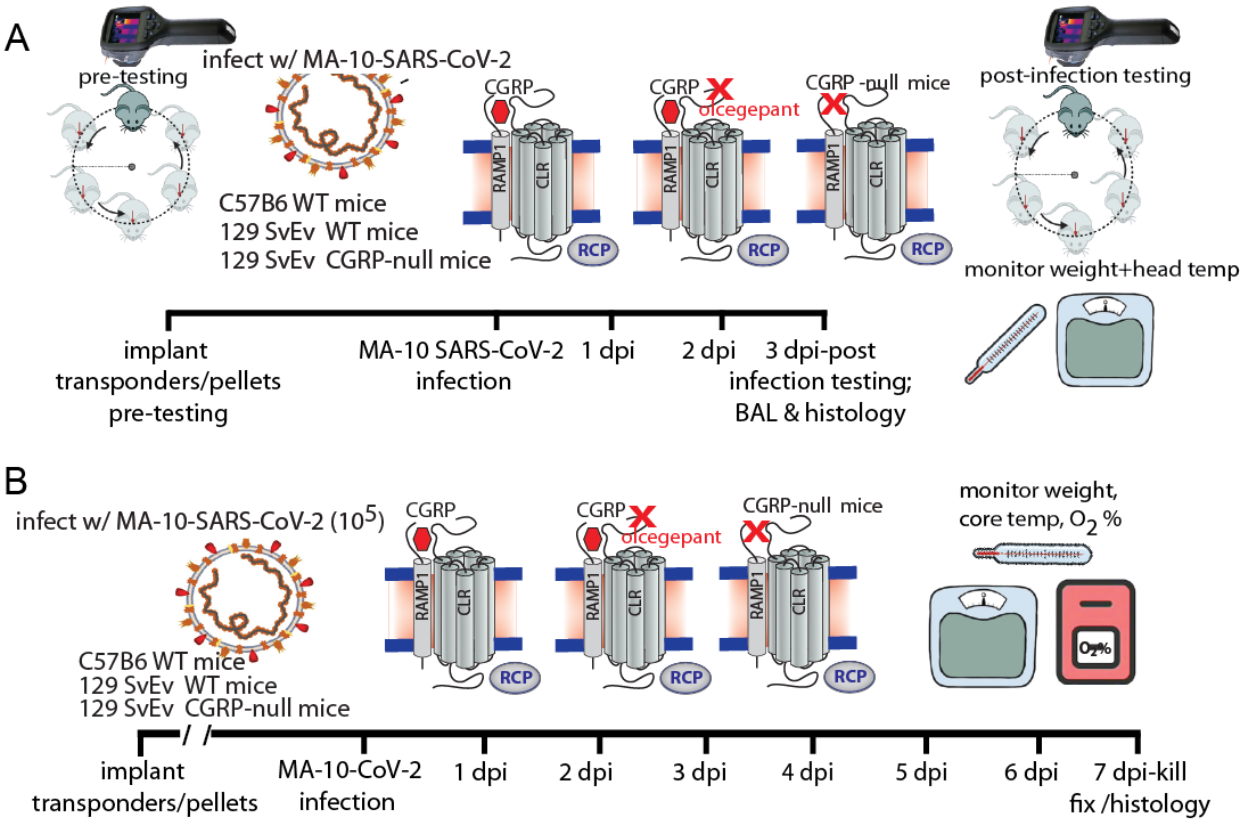

324

325

326 Fig. 1

327

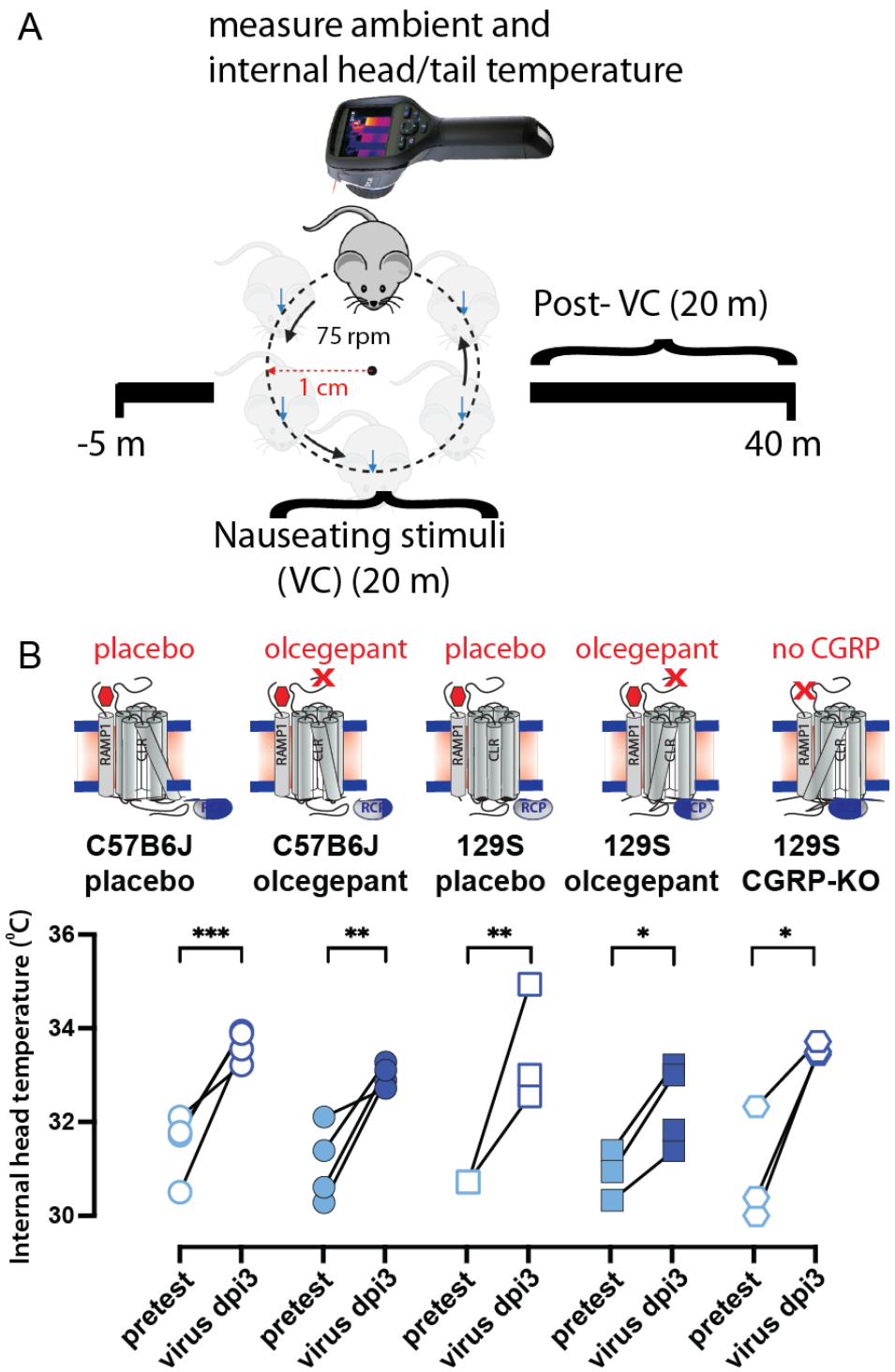
A
measure ambient and
internal head/tail temperature
75 rpm
1 cm
-5 m
Post- VC (20 m)
40 m
Nauseating stimuli
(VC) (20 m)
B
placebo
olcegepant
placebo
olcegepant
no CGRP
RAMP1
CLR
RCP
C57B6J
placebo
C57B6J
olcegepant
129S
placebo
129S
olcegepant
129S
CGRP-KO
Internal head temperature (°C)
36
34
32
30
***
**
**
*
*
pretest
virus dpi3

Fig. 2

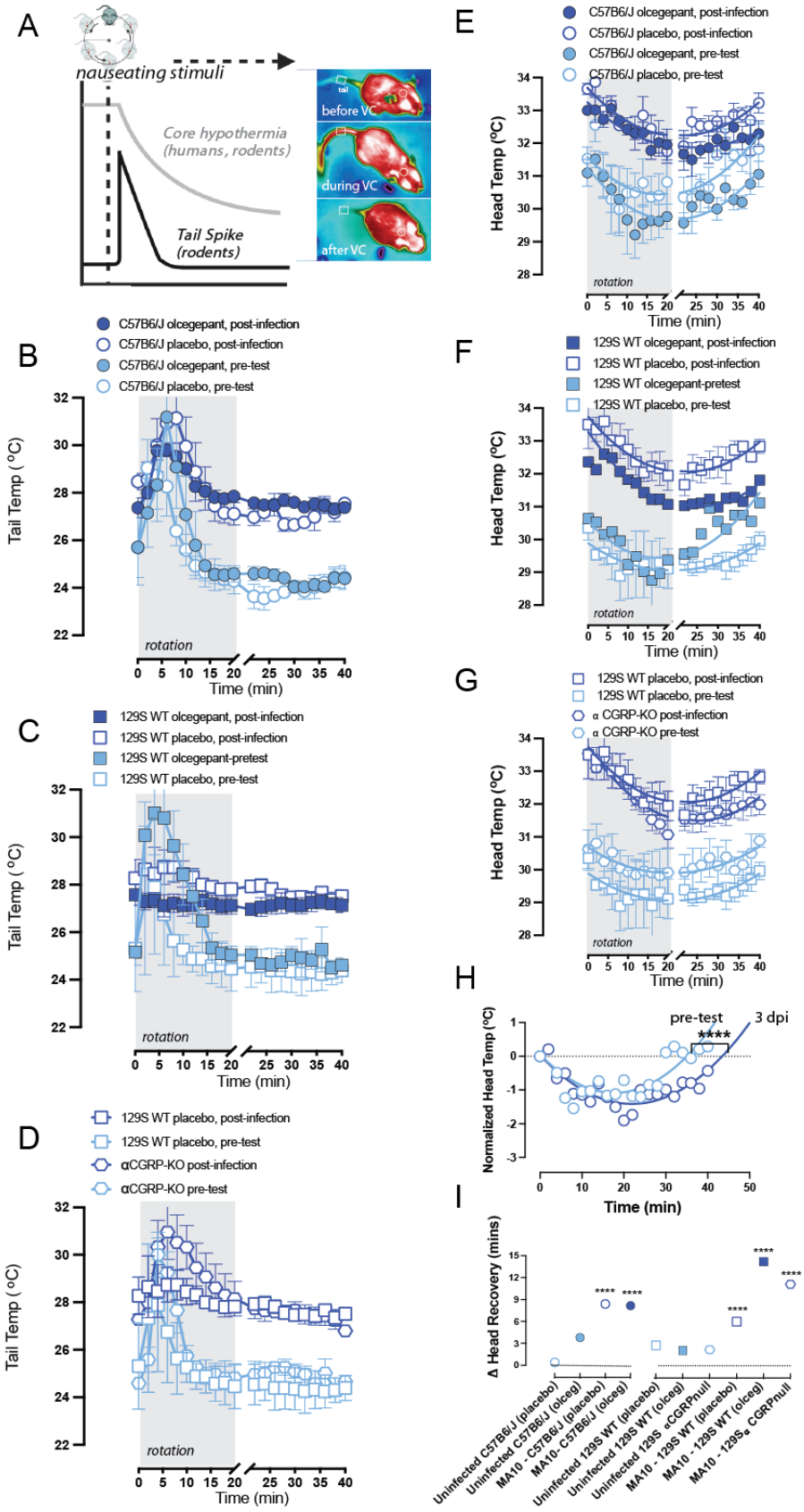
A
nauseating stimuli
Core hypothermia
(humans, rodents)
Tail Spike
(rodents)
before VC
during VC
after VC
B
C57B6/J olcegepant, post-infection
C57B6/J placebo, post-infection
C57B6/J olcegepant, pre-test
C57B6/J placebo, pre-test
Tail Temp (°C)
rotation
Time (min)
C
129S WT olcegepant, post-infection
129S WT placebo, post-infection
129S WT olcegepant-pretest
129S WT placebo, pre-test
Tail Temp (°C)
rotation
Time (min)
D
129S WT placebo, post-infection
129S WT placebo, pre-test
αCGRP-KO post-infection
αCGRP-KO pre-test
Tail Temp (°C)
rotation
Time (min)
E
C57B6/J olcegepant, post-infection
C57B6/J placebo, post-infection
C57B6/J olcegepant, pre-test
C57B6/J placebo, pre-test
Head Temp (°C)
rotation
Time (min)
F
129S WT olcegepant, post-infection
129S WT placebo, post-infection
129S WT olcegepant-pretest
129S WT placebo, pre-test
Head Temp (°C)
rotation
Time (min)
G
129S WT placebo, post-infection
129S WT placebo, pre-test
α CGRP-KO post-infection
α CGRP-KO pre-test
Head Temp (°C)
rotation
Time (min)
H
pre-test
3 dpi
****
Normalized Head Temp (°C)
Time (min)
I
Δ Head Recovery (mins)
Uninfected C57B6/J (placebo)
Uninfected C57B6/J (olceg)
MA10 - C57B6/J (placebo)
MA10- C57B6/J (olceg)
Uninfected 129S WT (placebo)
Uninfected 129S WT (olceg)
Uninfected 129S αCGRPnull
MA10 - 129S WT (placebo)
MA10 - 129S WT (olceg)
MA10 - 129Sα CGRPnull

Fig. 3

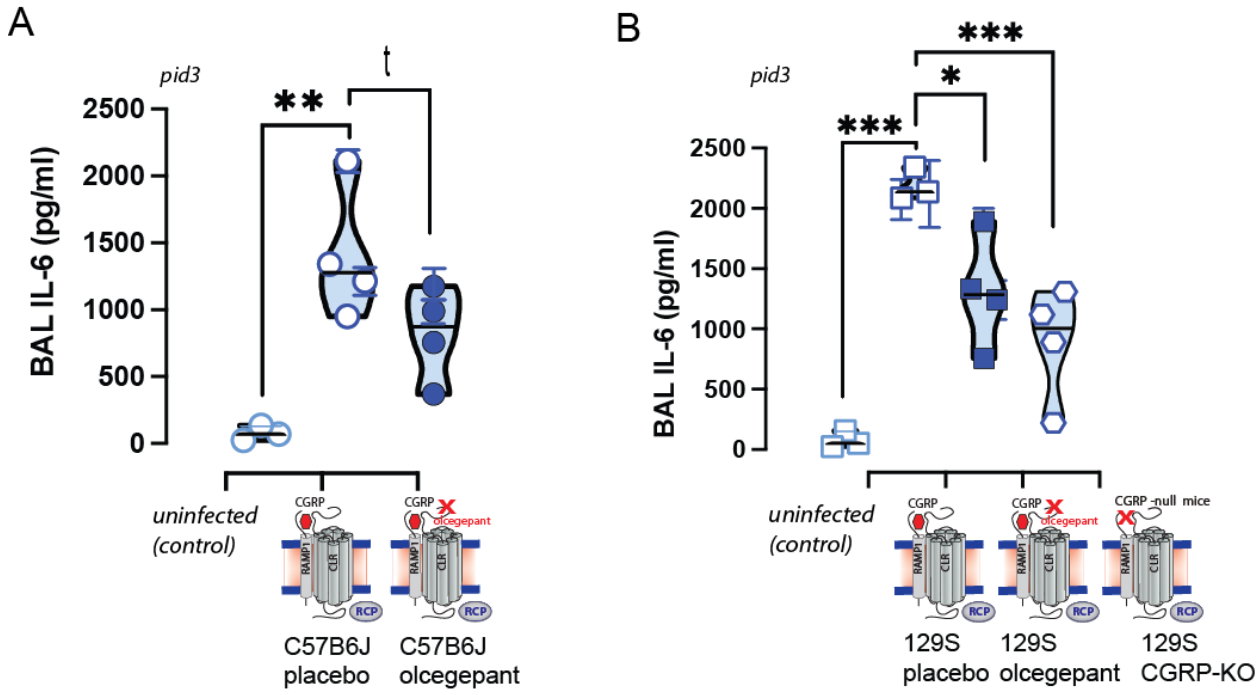
A
pid3
BAL IL-6 (pg/ml)
2500
2000
1500
1000
500
0
**
t
uninfected
(control)
CGRP
RAMP1
CLR
RCP
olcegepant
C57B6J
placebo
C57B6J
olcegepant
B
pid3
***
*
***
BAL IL-6 (pg/ml)
2500
2000
1500
1000
500
0
uninfected
(control)
CGRP
RAMP1
CLR
RCP
olcegepant
CGRP -null mice
129S
placebo
129S
olcegepant
129S
CGRP-KO

Fig. 4

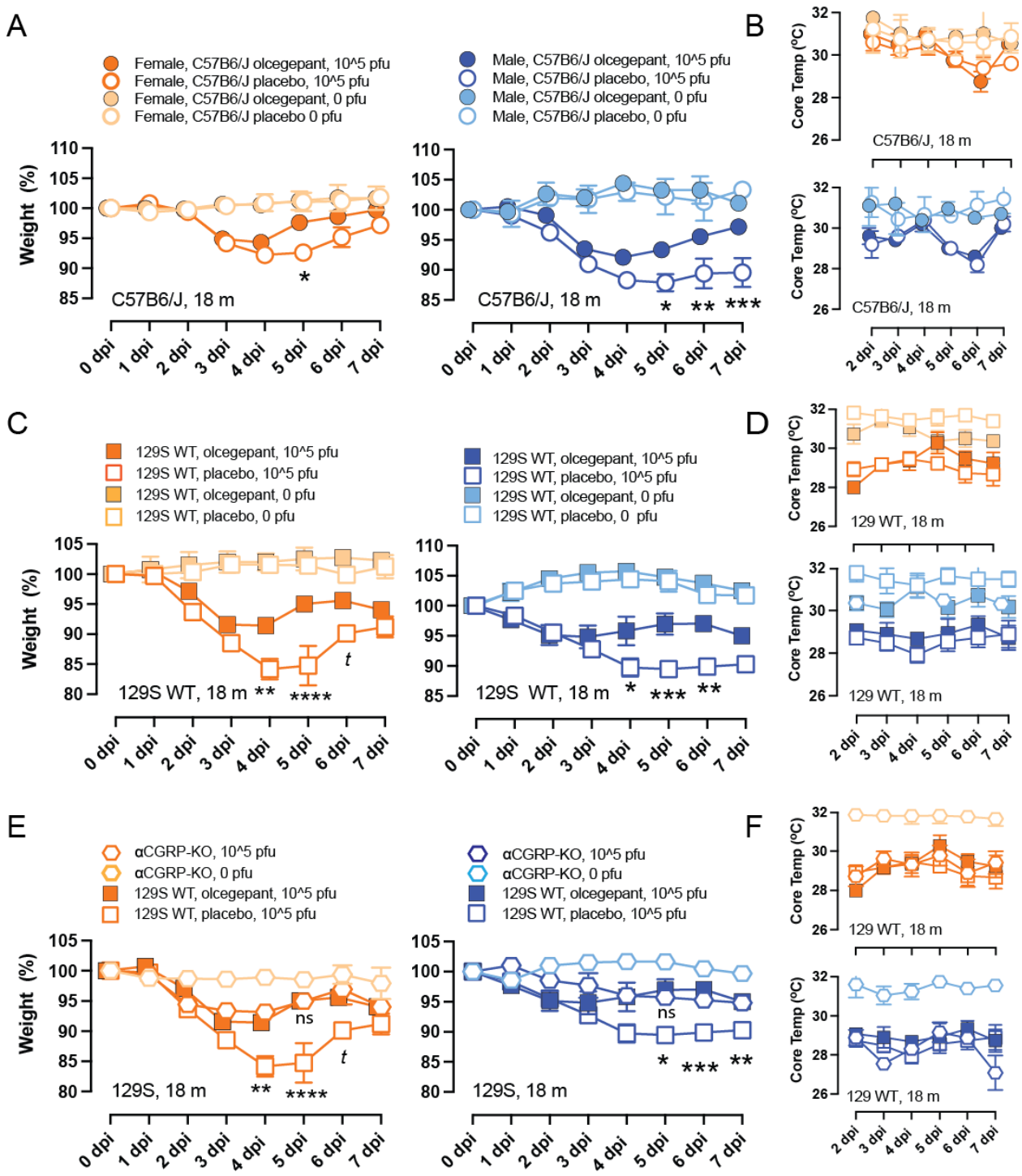
A
Female, C57B6/J olcegepant, 10^5 pfu
Female, C57B6/J placebo, 10^5 pfu
Female, C57B6/J olcegepant, 0 pfu
Female, C57B6/J placebo 0 pfu
Male, C57B6/J olcegepant, 10^5 pfu
Male, C57B6/J placebo, 10^5 pfu
Male, C57B6/J olcegepant, 0 pfu
Male, C57B6/J placebo, 0 pfu
Weight (%)
C57B6/J, 18 m
B
Core Temp (°C)
C
129S WT, olcegepant, 10^5 pfu
129S WT, placebo, 10^5 pfu
129S WT, olcegepant, 0 pfu
129S WT, placebo, 0 pfu
129S WT, 18 m
D
129 WT, 18 m
E
αCGRP-KO, 10^5 pfu
αCGRP-KO, 0 pfu
129S WT, olcegepant, 10^5 pfu
129S WT, placebo, 10^5 pfu
129S, 18 m
F
0 dpi
1 dpi
2 dpi
3 dpi
4 dpi
5 dpi
6 dpi
7 dpi

Fig. 5

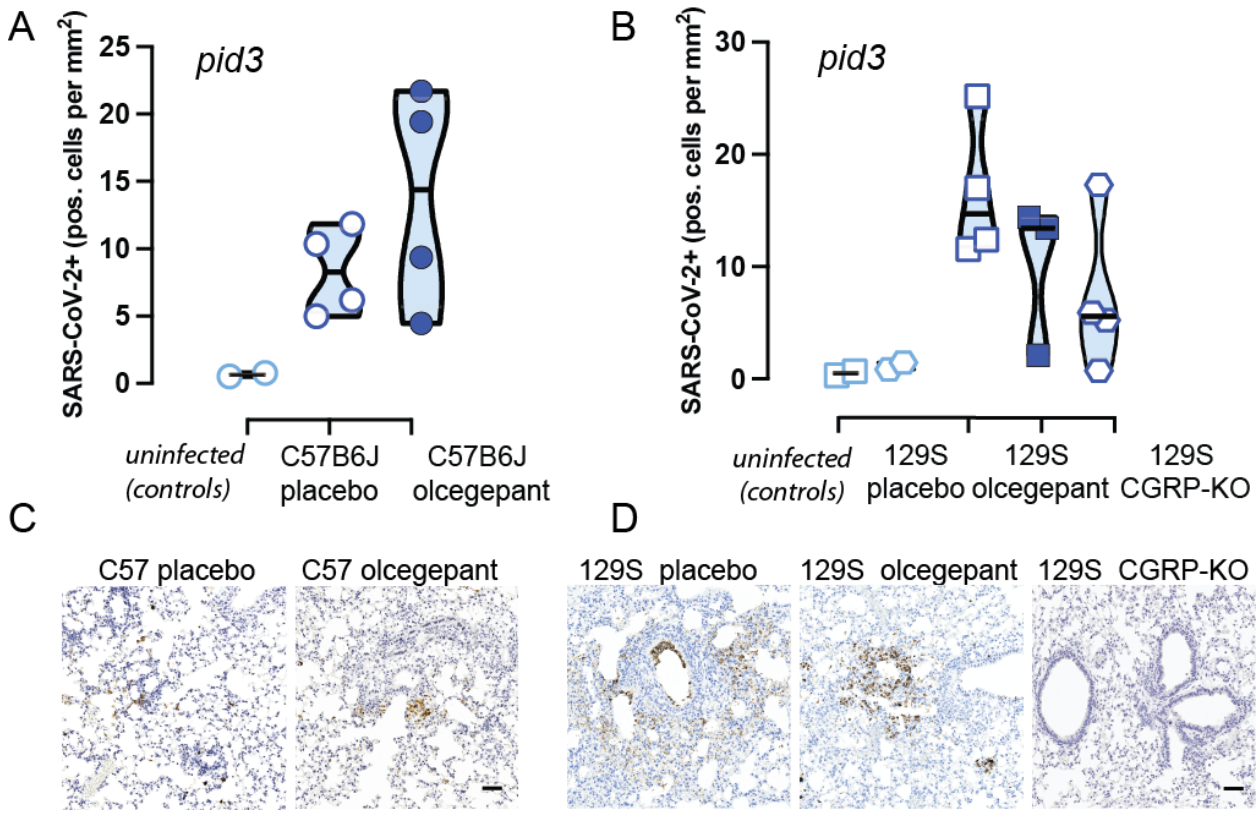
A
pid3
SARS-CoV-2+ (pos. cells per mm²)
25
20
15
10
5
0
uninfected (controls)
C57B6J placebo
C57B6J olcegepant
B
pid3
SARS-CoV-2+ (pos. cells per mm²)
30
20
10
0
uninfected (controls)
129S placebo
129S olcegepant
129S CGRP-KO
C
C57 placebo
C57 olcegepant
D
129S placebo
129S olcegepant
129S CGRP-KO

Fig. 6

359 **Figure Legends:**

360 **Fig. 1.** The study timelines are depicted. **A.** WT mice were infected with 10^5 pfu of MA-10
361 SARS-CoV-2 in the presence of placebo or CGRP-receptor antagonist olcegepant slow-release
362 pellets (olcegepant, BIBN4096, Tocris; 2 mg/kg/day/SQ) or mice lacking CGRP were infected
363 with the same virus; animals were then assessed for motion-induced nausea (dizziness) at 3
364 days after viral infection (dpi). At the completion of the nausea testing at 3dpi, bronchoalveolar
365 lavage (BAL) samples were collected for ELISA and lung tissue was obtained from control and
366 virus-infected animals at 3 dpi. Nausea (dizziness) was assessed for 45 minutes when mouse
367 was subjected to an orbital motion, noting temperature profiles (head and tail). **B.** WT mice
368 were infected with 10^5 pfu of MA-10 SARS-CoV-2 in the presence of placebo or CGRP-receptor
369 antagonist olcegepant slow-release pellets (olcegepant, BIBN4096, Tocris; 2 mg/kg/day/SQ) or
370 mice lacking CGRP were infected with the same virus; animals were then monitored for
371 changed in weight, core temperature and oxygen (O_2) saturation from 0 to 7 dpi.

372

373 **Fig. 2.** As shown in the **Fig 1A** timeline, older C57B/6, 129SvEv, and 129 mice lacking CGRP
374 were assessed for nausea (dizziness) when subjected to an orbital rotation, noting temperature
375 profiles (head and tail). **A.** Head and tail temperatures of mice were measured for a total 45
376 minutes using a FLIR E60 IR camera (model: E64501). This camera was connected to a tripod
377 and positioned approximately 43 cm above an open, plexiglass box (mouse box) used to house
378 an individual mouse during testing. Both the tripod and mouse box are securely attached to the
379 shaker's base. Briefly, baseline measurements were recorded for five minutes prior to the
380 provocative motion (-5 to 0 mins). The provocative motion was an orbital rotation (75 rpm, 2-cm
381 orbital displacement), and mice were recorded for 20 minutes (0 to 20 mins). After 20 minutes,
382 the provocative motion was turned off, and mice were recorded for an additional 20 minutes to
383 measure recovery to baseline (20 to 40 mins). Three mouse strains were tested: C57/B6J WT,
384 129S WT, and 129S αCGRP-null mice. Within each wild type (WT) strain, four groups of mice

385 were tested: placebo only, olcegepant only, placebo with 10^5 MA-SARS-CoV-2, and olcegepant
386 with 10^5 SARS-CoV-2 MA-10. Virus-infected mice were tested at Cornell University's ABSL-3
387 environment, with all pre-infection testing performed at University of Rochester. **B.** All tested
388 mice experienced a fever-like state 3 days post-viral infection (3 dpi). Olcegepant did not have a
389 protective effect in reducing this acute fever-like state at 3 dpi.

390

391 **Fig. 3. A.** Upon provocative motion, humans and mice will show a drop in head temperature
392 that recovers once rotation is ceased, and mice show a transient tail spike ~10 min into rotation.
393 When nausea or dizziness is present, the head temperature drop takes longer to recover, and
394 the transient tail spike diminishes or disappears. **B,C,D.** Viral infection diminishes tail
395 vasodilatations and impairs a mouse's natural response to the provocative motion. At time t = 0,
396 mice experience a 20-minute provocative motion and exhibit a significant increase in tail
397 temperature. Δ tails are computed and are corrected for ambient temperature. Findings suggest
398 that olcegepant did not protect against virus-induced changes in tail vasodilation at 3 dpi in all of
399 the strains tested. **E,F,G.** Viral infection impacts recovery from hypothermia after provocative
400 motion. **H.** Second order curve fits observed recovery of head temperatures after provocative
401 motion to baseline. Across all strains, mice experienced delayed temperature recovery
402 compared to pretest, with longer recovery profiles. **I.** No protective effects were seen by
403 olcegepant in temperature recovery for any of the tested strains.

404

405

406 **Fig. 4.** Bronco-alveolar lavage (BAL) samples were obtained for ELISA testing, and lungs were
407 obtained for subsequent immunohistochemistry at 3 dpi. MA-SARS-CoV-2 infection increased
408 the release of the inflammatory cytokine IL-6, and this IL-6 release was attenuated by CGRP
409 signaling blockade. In both C57B6/J **(A)** and 129S mice **(B)** strains, IL-6 release was

410 attenuated by olcegepant SQ release. Moreover, in αCGRP null mice, IL-6 cytokine release was
411 statistically equivalent to non-infected controls **(B)**.
412
413 **Fig. 5.** Older (18 months) female and male mice were tested for weight loss and core
414 temperature drops after infection with MA-10 SARS-CoV-2, 10^5 pfu virus at 0-7 dpi. **A. C.** We
415 found that animals treated with olcegepant recovered from the initial weight loss, with male mice
416 showing increased protection. **A.** C57B6/J; **C.** 129S. **E.** Similar to the IL-6 findings (**Fig. 4**),
417 mice lacking the CGRP peptide were not significantly different from uninfected controls. **B, D,**
418 **F.** Viral infection caused core temperatures of mice to decrease, and this effect was unaltered
419 by olcegepant treatment.
420
421 **Fig. 6.** A**&B.** There was no statistically significant difference in the number of SARS-CoV-2
422 antigen-positive cells in the lungs of (**A, C**) C57/B6J or (**B, D**) 129 mice, between mice that
423 received placebo versus olcegepant pellets at 3 dpi. **C, D.** Representative SARS-CoV-2
424 immunostaining is shown for 3 dpi lung issues from C57B6/J (**C**), and 129S (**D**) mice. Scale bar
425 is 100 μm. (*= $p < 0.05$, ** =$p < 0.01$, ** *= $p < 0.001$, **** = $p < 0.0001$)
426

427 **References:**

428 Abobaker, A., and M. Darrat. 2021. 'Letter to the Editor From Abobaker and Darrat: "Circulating
429 Levels of Calcitonin Gene-Related Peptide Are Lower in COVID-19 Patients"', *J Endocr*
430 *Soc*, 5: bvab052.

431 Achanta, R., A. Shaji, K. Smith, A. Lucchi, P. Fua, and S. Susstrunk. 2012. 'SLIC superpixels
432 compared to state-of-the-art superpixel methods', *IEEE Trans Pattern Anal Mach Intell*,
433 34: 2274-82.

434 Aghagoli, G., B. Gallo Marin, N. J. Katchur, F. Chaves-Sell, W. F. Asaad, and S. A. Murphy.
435 2021. 'Neurological Involvement in COVID-19 and Potential Mechanisms: A Review',
436 *Neurocrit Care*, 34: 1062-71.

437 Assas, B. M., J. A. Miyan, and J. L. Pennock. 2014. 'Cross-talk between neural and immune
438 receptors provides a potential mechanism of homeostatic regulation in the gut mucosa',
439 *Mucosal Immunol*, 7: 1283-9.

440 Assas, B. M., J. I. Pennock, and J. A. Miyan. 2014. 'Calcitonin gene-related peptide is a key
441 neurotransmitter in the neuro-immune axis', *Front Neurosci*, 8: 23.

442 Bankhead, P., M. B. Loughrey, J. A. Fernandez, Y. Dombrowski, D. G. McArt, P. D. Dunne, S.
443 McQuaid, R. T. Gray, L. J. Murray, H. G. Coleman, J. A. James, M. Salto-Tellez, and P.
444 W. Hamilton. 2017. 'QuPath: Open source software for digital pathology image analysis',
445 *Sci Rep*, 7: 16878.

446 Bohn, M. K., A. Hall, L. Sepiashvili, B. Jung, S. Steele, and K. Adeli. 2020. 'Pathophysiology of
447 COVID-19: Mechanisms Underlying Disease Severity and Progression', *Physiology*
448 *(Bethesda)*, 35: 288-301.

449 Bolay, H., O. Karadas, B. Ozturk, R. Sonkaya, B. Tasdelen, T. D. S. Bulut, O. Gulbahar, A.
450 Ozge, and B. Baykan. 2021. 'HMGB1, NLRP3, IL-6 and ACE2 levels are elevated in
451 COVID-19 with headache: a window to the infection-related headache mechanism', *J*
452 *Headache Pain*, 22: 94.

453 Caronna, E., V. Jose Gallardo, A. Alpuente, M. Torres-Ferrus, N. M. Sanchez-Mateo, J.
454 Viguera-Romero, A. C. Lopez-Veloso, A. Lopez-Bravo, A. B. Gago-Veiga, P. Irimia
455 Sieira, J. Porta-Etessam, S. Santos-Lasaosa, P. Pozo-Rosich, and Cgrp-Covid Study
456 Group Spanish. 2021. 'Safety of anti-CGRP monoclonal antibodies in patients with
457 migraine during the COVID-19 pandemic: Present and future implications', *Neurologia*
458 *(Engl Ed)*, 36: 611-17.

459 Channappanavar, R., and S. Perlman. 2017. 'Pathogenic human coronavirus infections: causes
460 and consequences of cytokine storm and immunopathology', *Semin Immunopathol*, 39:
461 529-39.

462 Del Vecchio, F., E. Nalivaiko, M. Cerri, M. Luppi, and R. Amici. 2014. 'Provocative motion
463 causes fall in brain temperature and affects sleep in rats', *Exp Brain Res*, 232: 2591-9.

464 Dinnon, K. H., 3rd, S. R. Leist, A. Schafer, C. E. Edwards, D. R. Martinez, S. A. Montgomery, A.
465 West, B. L. Yount, Jr., Y. J. Hou, L. E. Adams, K. L. Gully, A. J. Brown, E. Huang, M. D.
466 Bryant, I. C. Choong, J. S. Glenn, L. E. Gralinski, T. P. Sheahan, and R. S. Baric. 2020.
467 'A mouse-adapted model of SARS-CoV-2 to test COVID-19 countermeasures', *Nature*,
468 586: 560-66.

469 ———. 2021. 'Publisher Correction: A mouse-adapted model of SARS-CoV-2 to test COVID-19
470 countermeasures', *Nature*, 590: E22.

471 Dinnon, K. H., S. R. Leist, K. Okuda, H. Dang, E. J. Fritch, K. L. Gully, G. De la Cruz, M. D.
472 Evangelista, T. Asakura, R. C. Gilmore, P. Hawkins, S. Nakano, A. West, A. Schafer, L.

473 E. Gralinski, J. L. Everman, S. P. Sajuthi, M. R. Zweigart, S. Dong, J. McBride, M. R.
474 Cooley, J. B. Hines, M. K. Love, S. D. Groshong, A. VanSchoiack, S. J. Phelan, Y.
475 Liang, T. Hether, M. Leon, R. E. Zumwalt, L. M. Barton, E. J. Duval, S. Mukhopadhyay,
476 E. Stroberg, A. Borczuk, L. B. Thorne, M. K. Sakthivel, Y. Z. Lee, J. S. Hagood, J. R.
477 Mock, M. A. Seibold, W. K. O'Neal, S. A. Montgomery, R. C. Boucher, and R. S. Baric.
478 2022. 'A model of persistent post SARS-CoV-2 induced lung disease for target
479 identification and testing of therapeutic strategies', *bioRxiv*.

480 Doods, H., G. Hallermayer, D. Wu, M. Entzeroth, K. Rudolf, W. Engel, and W. Eberlein. 2000.
481 'Pharmacological profile of BIBN4096BS, the first selective small molecule CGRP
482 antagonist', *Br J Pharmacol*, 129: 420-3.

483 Grassini, A., A. Marcinno, F. Roveta, E. Gallo, A. Cermelli, S. Boschi, E. Rubino, and I. Rainero.
484 2021. 'Impact of COVID-19 on chronic migraine treated with erenumab: a case report',
485 *Neurol Sci*, 42: 3079-81.

486 Han, D. 2019. 'Association of Serum Levels of Calcitonin Gene-related Peptide and Cytokines
487 during Migraine Attacks', *Ann Indian Acad Neurol*, 22: 277-81.

488 Karadas, O., B. Ozturk, A. R. Sonkaya, B. Tasdelen, A. Ozge, and H. Bolay. 2021. 'Latent class
489 cluster analysis identified hidden headache phenotypes in COVID-19: impact of
490 pulmonary infiltration and IL-6', *Neurol Sci*, 42: 1665-73.

491 Kuba, K., Y. Imai, S. Rao, H. Gao, F. Guo, B. Guan, Y. Huan, P. Yang, Y. Zhang, W. Deng, L.
492 Bao, B. Zhang, G. Liu, Z. Wang, M. Chappell, Y. Liu, D. Zheng, A. Leibbrandt, T. Wada,
493 A. S. Slutsky, D. Liu, C. Qin, C. Jiang, and J. M. Penninger. 2005. 'A crucial role of
494 angiotensin converting enzyme 2 (ACE2) in SARS coronavirus-induced lung injury', *Nat
495 Med*, 11: 875-9.

496 Littlefield, K. M., R. O. Watson, J. M. Schneider, C. P. Neff, E. Yamada, M. Zhang, T. B.
497 Campbell, M. T. Falta, S. E. Jolley, A. P. Fontenot, and B. E. Palmer. 2022. 'SARS-CoV-
498 2-specific T cells associate with inflammation and reduced lung function in pulmonary
499 post-acute sequalae of SARS-CoV-2', *PLoS Pathog*, 18: e1010359.

500 Liu, Y., C. Zhang, F. Huang, Y. Yang, F. Wang, J. Yuan, Z. Zhang, Y. Qin, X. Li, D. Zhao, S. Li,
501 S. Tan, Z. Wang, J. Li, C. Shen, J. Li, L. Peng, W. Wu, M. Cao, L. Xing, Z. Xu, L. Chen,
502 C. Zhou, W. J. Liu, L. Liu, and C. Jiang. 2020. 'Elevated plasma levels of selective
503 cytokines in COVID-19 patients reflect viral load and lung injury', *Natl Sci Rev*, 7: 1003-
504 11.

505 Mallee, J. J., C. A. Salvatore, B. LeBourdelles, K. R. Oliver, J. Longmore, K. S. Koblan, and S.
506 A. Kane. 2002. 'Receptor activity-modifying protein 1 determines the species selectivity
507 of non-peptide CGRP receptor antagonists', *J Biol Chem*, 277: 14294-8.

508 Mazloumi Gavgani, A., D. M. Hodgson, and E. Nalivaiko. 2017. 'Effects of visual flow direction
509 on signs and symptoms of cybersickness', *PLoS One*, 12: e0182790.

510 Ngampramuan, S., M. Cerri, F. Del Vecchio, J. J. Corrigan, A. Kamphee, A. S. Dragic, J. A.
511 Rudd, A. A. Romanovsky, and E. Nalivaiko. 2014. 'Thermoregulatory correlates of
512 nausea in rats and musk shrews', *Oncotarget*, 5: 1565-75.

513 Ochoa-Callejero, L., J. Garcia-Sanmartin, P. Villoslada-Blanco, M. Iniguez, P. Perez-Matute, E.
514 Pujadas, R. Brody, J. A. Oteo, and A. Martinez. 2021. 'Response to Letter to the Editor
515 from Abobaker and Darrat: "Circulating levels of Calcitonin Gene-Related Peptide Are
516 Lower in COVID-19 Patients"', *J Endocr Soc*, 5: bvab053.

517 Ozkan, E., O. Celebi, O. Keskin, A. Gursoy, and Y. Gursoy-Ozdemir. 2022. 'Is Persistent Post-
518 COVID Headache Associated With Protein-Protein Interactions Between Antibodies

519 Against Viral Spike Protein and CGRP Receptor?: A Case Report', *Front Pain Res*
520 *(Lausanne)*, 3: 858709.

521 Rizzi, M., S. Tonello, F. Morani, E. Rizzi, G. F. Casciaro, E. Matino, M. Costanzo, E. Zecca, A.
522 Croce, A. Pedrinelli, V. Vassia, R. Landi, V. R. Mallela, D. D'Onghia, R. Minisini, M.
523 Bellan, L. M. Castello, F. Gavelli, G. C. Avanzi, F. Patrucco, M. Pirisi, D. Colangelo, and
524 P. P. Sainaghi. 2022. 'CGRP Plasma Levels Correlate with the Clinical Evolution and
525 Prognosis of Hospitalized Acute COVID-19 Patients', *Viruses*, 14.

526 Robertson, C. E. 2020. 'Could CGRP antagonists be helpful in the fight against COVID-19?',
527 *Headache*.

528 Romano, F., N. Caramia, D. Straumann, E. Nalivaiko, and G. Bertolini. 2017. 'Cross-coupling
529 vestibular stimulation: motion sickness and the vestibulo-sympathetic reflex', *J Neurol*.

530 Saniasiaya, J., and J. Kulasegarah. 2021. 'Dizziness and COVID-19', *Ear Nose Throat J*, 100:
531 29-30.

532 Shapira, T., I. A. Monreal, S. P. Dion, D. W. Buchholz, B. Imbiakha, A. D. Olmstead, M. Jager,
533 A. Desilets, G. Gao, M. Martins, T. Vandal, C. A. H. Thompson, A. Chin, W. D. Rees, T.
534 Steiner, I. R. Nabi, E. Marsault, J. Sahler, D. G. Diel, G. R. Van de Walle, A. August, G.
535 R. Whittaker, P. L. Boudreault, R. Leduc, H. C. Aguilar, and F. Jean. 2022. 'A TMPRSS2
536 inhibitor acts as a pan-SARS-CoV-2 prophylactic and therapeutic', *Nature*, 605: 340-48.

537 Shapira, T., I. A. Monreal, S. P. Dion, M. Jager, A. Desilets, A. D. Olmstead, T. Vandal, D. W.
538 Buchholz, B. Imbiakha, G. Gao, A. Chin, W. D. Rees, T. Steiner, I. R. Nabi, E. Marsault,
539 J. Sahler, A. August, G. Van de Walle, G. R. Whittaker, P. L. Boudreault, H. C. Aguilar,
540 R. Leduc, and F. Jean. 2021. 'A novel highly potent inhibitor of TMPRSS2-like proteases
541 blocks SARS-CoV-2 variants of concern and is broadly protective against infection and
542 mortality in mice', *bioRxiv*.

543 Tu, L., L. Poppi, J. Rudd, E. T. Cresswell, D. W. Smith, A. Brichta, and E. Nalivaiko. 2017.
544 'Alpha-9 nicotinic acetylcholine receptors mediate hypothermic responses elicited by
545 provocative motion in mice', *Physiol Behav*, 174: 114-19.

546 Zhu, N., D. Zhang, W. Wang, X. Li, B. Yang, J. Song, X. Zhao, B. Huang, W. Shi, R. Lu, P. Niu,
547 F. Zhan, X. Ma, D. Wang, W. Xu, G. Wu, G. F. Gao, W. Tan, Investigating China Novel
548 Coronavirus, and Team Research. 2020. 'A Novel Coronavirus from Patients with
549 Pneumonia in China, 2019', *N Engl J Med*, 382: 727-33.

550 Ziegler, C. G. K., S. J. Allon, S. K. Nyquist, I. M. Mbano, V. N. Miao, C. N. Tzouanas, Y. Cao, A.
551 S. Yousif, J. Bals, B. M. Hauser, J. Feldman, C. Muus, M. H. Wadsworth, 2nd, S. W.
552 Kazer, T. K. Hughes, B. Doran, G. J. Gatter, M. Vukovic, F. Taliaferro, B. E. Mead, Z.
553 Guo, J. P. Wang, D. Gras, M. Plaisant, M. Ansari, I. Angelidis, H. Adler, J. M. S. Sucre,
554 C. J. Taylor, B. Lin, A. Waghray, V. Mitsialis, D. F. Dwyer, K. M. Buchheit, J. A. Boyce,
555 N. A. Barrett, T. M. Laidlaw, S. L. Carroll, L. Colonna, V. Tkachev, C. W. Peterson, A.
556 Yu, H. B. Zheng, H. P. Gideon, C. G. Winchell, P. L. Lin, C. D. Bingle, S. B. Snapper, J.
557 A. Kropski, F. J. Theis, H. B. Schiller, L. E. Zaragosi, P. Barbry, A. Leslie, H. P. Kiem, J.
558 L. Flynn, S. M. Fortune, B. Berger, R. W. Finberg, L. S. Kean, M. Garber, A. G. Schmidt,
559 D. Lingwood, A. K. Shalek, J. Ordovas-Montanes, H. C. A. Lung Biological Network.
560 Electronic address: lung-network@humancellatlas.org, and H. C. A. Lung Biological
561 Network. 2020. 'SARS-CoV-2 Receptor ACE2 Is an Interferon-Stimulated Gene in
562 Human Airway Epithelial Cells and Is Detected in Specific Cell Subsets across Tissues',
563 *Cell*.
564